Protein WW domain denaturation on defective graphene reveals the significance of nanomaterial defects in nanotoxicity

Baoyu Li [a], David R. Bell [b], Zonglin Gu [a], Weifeng Li [c, *], Ruhong Zhou [a, b, d, **]

[a] Institute of Quantitative Biology and Medicine, State Key Laboratory of Radiation Medicine and Protection, School of Radiation Medicine and Protection, Collaborative Innovation Center of Radiation Medicine of Jiangsu Higher Education Institutions, Soochow University, Suzhou 215123, China
[b] Computational Biological Center, IBM Thomas J. Watson Research Center, Yorktown Heights, NY 10598, USA
[c] School of Physics and State Key Laboratory of Crystal Materials, Shandong University, Jinan 250100, China
[d] Department of Chemistry, Columbia University, New York, NY 10027, USA

ARTICLE INFO

ABSTRACT

Nanomaterial defects occur widely due to various situations such as synthesis imperfections, exposure to harsh environment, or even intentional designs. However, the consequence of nanomaterial defects on their interfacing biological systems remains largely unknown. Here, we study the interaction of a defective graphene nanosheet with a widely used model protein, YAP65WW-domain, using molecular dynamics simulations. We find that local defects on graphene consistently act to unfold the YAP65WW-domain. Protein residues bound to the graphene defect are tightly anchored due to favorable electrostatic interactions. While the residues at the interface are highly restrained, thermal movements of other parts of the protein act to denature and unfold the entire protein. In contrast, control simulations of protein binding on ideal graphene reveal a well preserved native structure with no unfolding events detected. Our present findings elucidate the role of graphene defects on protein adsorption and emphasize the need for improved understanding of nanomaterial defects in potential biomedical applications.

© 2019 Elsevier Ltd. All rights reserved.

1. Introduction

With the rapid development of nanotechnology and nanoscience, nanomaterials especially carbon based nanomaterials (such as graphene, fullerene and carbon nanotubes) have attracted extensive interest due to their extraordinary chemical and physical properties [1—5]. In addition to the development of electronic devices utilizing these unique properties, carbon based nanomaterials have also been applied to the biomedical field, yielding diverse employment as drug and gene delivery platforms, cell/tissue labeling and imaging agents, tumor photothermal and photodynamic therapies [6—13].

Despite the increasing prevalence of nanomaterials in biomedical applications, the primary concern of biosafety, or cytotoxicity, of the nanomaterials have also attracted great research interest. It has been widely reported that nanomaterials can enter cells and accumulate in the cytoplasm, causing lung injury, immunotoxicity, and adverse cardiovascular dysfunction [14—19]. Given their reduced dimensions, nanomaterials have a large surface to volume ratio leading to substantial exposure and interaction with biomolecules. For instance, recent studies indicated that nanomaterials (including carbon nanotubes and fullerene) are able to block ion channel proteins and affect their putative functions [20,21]. Our previous studies have demonstrated that nanomaterials (graphene and WS_2 nanosheet) can cause severe integrity distortions of cell membrane through extracting large amounts of phospholipids from the cell membranes, which effectively cause cell death [22,23].

Because of the preparation process used and the environmental and operating conditions, it is inevitable that experimentally fabricated nanomaterials are imperfect and contain defects. Defects may cause unwanted changes to the electronic and mechanical changes of nanomaterials, or in some cases, defects lead to desired functionalities. Taking the prototype 2D material — graphene — for example, graphene with defects can be used in nanoelectronics for opening a band gap [24]. Being used as nano-filters, graphene with proper sized defects can be used as high performance DNA-

* Corresponding author.
** Corresponding author. Institute of Quantitative Biology and Medicine, State Key Laboratory of Radiation Medicine and Protection, School of Radiation Medicine and Protection, Collaborative Innovation Center of Radiation Medicine of Jiangsu Higher Education Institutions, Soochow University, Suzhou 215123, China.
E-mail addresses: lwf@sdu.edu.cn (W. Li), ruhongz@us.ibm.com (R. Zhou).

sequencing devices or sieving membranes for gas separation and seawater desalination [24–27]. For biological interactions, the characteristics of nanomaterial surfaces determine how they bind to, and regulate the structure of biomolecules. Thus, understanding defects of nanomaterials could be a promising solution for the design of functional bio-nanomaterials. Although the interactions between biomolecules and nanomaterials have been widely studied by experimental and theoretical approaches [28,29], for example, Guo et al. systematically studied the interaction of several small proteins with idealized graphene [30], the contribution from defects has yet to be studied, exposing an urgent need for a comprehensive understanding of how defects influence biological interactions.

In this work, we systematically investigate the adsorption of a WW-domain (YAP65WW) onto a graphene monolayer with local defects (D-Gra) using molecular dynamics simulations. We selected the WW domain as our model protein due to its seminal role and ubiquitous involvement in signaling and regulatory pathways. The WW domain recognizes the proline-rich motifs (PRMs) in signal transduction and is involved in the control of epithelial sodium channels. It also has implications in several human diseases including Alzheimer's disease [31,32]. Moreover, it has been widely used as a model protein in many previous studies on protein folding kinetics and protein interactions with nanomaterials [33,34]. We compare defected graphene adsorption to the control of ideal graphene (I-Gra) adsorption. The simulations reveal that both D-Gra and I-Gra attract and adsorb YAP65WW to form stable binding. Notably, upon binding to D-Gra, YAP65WW experiences drastic structural deformations, losing most of its secondary and tertiary structures. We observe the charged residues of YAP65WW to form strong, specific interactions with the graphene defects and become immobilized. Due to the thermal motion of the global protein, YAP65WW then unfolds from these immobilized residues. In contrast, I-Gra demonstrated much weaker toxicity to YAP65WW with only a slight impact on its native structure. Our findings reveal the important, varied consequences of nanomaterial defects in nano-bio interactions and the need for comprehensive understanding in applying nanomaterials to biological systems.

2. Simulation methods

The initial coordinates of the YAP65WW protein domain were obtained from the crystal structure (PDB code 1JMQ [35] with the L30K mutation left intact and truncated to include residues 15-40[33]) and modeled by CHARMM27 force field [36]. Its native state exists as a triple-stranded, antiparallel β-sheet structure as shown in Fig. 1b. The I-Gra nanosheet with dimensions of 12.53×12.76 nm^2 was generated using the nanotube builder plugin of VMD software [37]. The carbon atoms of graphene were modeled as uncharged Lennard-Jones particles with a cross section of $\sigma_{cc} = 0.34$ nm and a potential well depth of $\varepsilon_{cc} = 0.36$ kJ/mol [38,39]. For D-Gra shown in Fig. 1a, nine defects (diameter around 1 nm) were inserted into the I-Gra nanosheet. The defect edges comprise twelve C atoms that are saturated by alternative charged carboxyl groups and hydrogen atoms. More details about the Lennard-Jones parameters and atomic charges for the D-Gra model can be found in Table S1 in the Supplementary Information (SI). Following our previous study [40], the positions of D-Gra and I-Gra nanosheet were restrained using a harmonic potential with force constant of 1000 kJ mol^{-1} nm^{-2} in all the simulations. Under this condition, the atoms of D-Gra and I-Gra can still fluctuate in the simulations to mimic more closely to the local surface curvatures. In the simulation, the YAP65WW protein was initially placed parallel to the D-Gra/I-Gra nanosheet with a separation of 1.26 nm. The YAP65WW/Gra complex was solvated in a cubic water box with periodic boundary conditions in all directions. Solvent was modeled explicitly with the TIP3P water model [41]. To neutralize the systems, 53 Na$^+$ atoms were added to the protein-D-Gra system and 1 Cl$^-$ atoms was added to the protein-I-Gra system. The detailed contents of two simulation systems are summarized in Table S2 in the SI.

MD simulations were performed using the GROMACS-4.6.6 package [42]. The electrostatic interactions were treated using the particle mesh Ewald (PME) method [43,44] (using fourth-order interpolation and the maximum Fourier spacing for the FFT grid is 0.1 nm), while van der Waals interactions were calculated with a cutoff distance of 1.2 nm. Covalent bond lengths involving hydrogen atoms were constrained by the LINCS algorithm [45]. After energy minimization, all simulations were equilibrated for 500 ps in the NVT ensemble using v-rescale thermostat [46] at 300 K. After that, 500 ns production simulations were conducted at a constant pressure of 1 bar and a temperature of 300 K using the Berendsen coupling method [47]. For D-Gra and I-Gra respectively, three independent production simulations with different initial YAP65WW orientations were conducted to yield a total simulation time of over 3 μs.

3. Results and discussions

3.1. Structural evolution of YAP65WW upon binding onto D-Gra and I-Gra

In the initial system configuration, YAP65WW is separated from the graphene sheets by 1.26 nm, as shown in Fig. 1a. YAP65WW diffuses and contacts the graphene surface within tens of ns and adsorbs onto the graphene nanosheet in all six trajectories. Despite the timely adsorption onto both defective and ideal graphene nanosheet, the YAP65WW was found to adopt distinct conformations when interacting with two graphene models. In the D-Gra simulations, the YAP65WW domain experienced drastic structural distortions and completely unfolded from its native structure (Fig. 1c-e). We observed several key residues at the YAP65WW/D-Gra interface (highlighted as sticks in Fig. 1c-e): the Lys-7 formed direct contacts with the defects, while three aromatic residues, Trp-3, Phe-15 and Trp-25, bind to the defect-free regions of D-Gra, forming the face-to-face π-π stacking. In contrast, for the I-Gra simulations, no obvious distortion or unfolding of YAP65WW was detected beyond slight changes at the two termini (Fig. 1f-h). From previous studies of nanomaterial toxicity, it is generally accepted that protein conformation changes upon interacting with nanomaterials are one of the main reasons for the nanotoxicity [40,48]. As mentioned above, YAP65WW is a ubiquitous protein domain involved in signaling and regulation pathways, and its conformation, particularly its proline-rich-motif (PMF) binding groove, is critical for its function. Thus, the drastic structural distortions caused by D-Gra indicates a potential role of the defects in the toxicity of graphene materials.

Fig. 2 depicts some representative patterns of how YAP65WW unfolds upon binding to D-Gra surface. The protein approached to the vicinity of the D-Gra surface at ~6 ns after which the positively charged Arg-13 began to form direct contact with the negatively charged oxygen atoms of D-Gra (Fig. 2b) through electrostatic interactions. It is found that during the rest of the simulations, Arg-13 was always tightly "anchored" at the defect region, while other parts of the protein still migrated along the transverse directions on D-Gra surface. At about 45 ns (Fig. 2c), Phe-15 and Trp-25 formed π–π stacking with D-Gra, and the YAP65WW began to unfold which initiated at the β-sheet 3 segment. At ~108 ns (Fig. 2d), the YAP65WW was fully unfolded, with Trp-3 forming π–π stacking with D-Gra as well. The unfolded conformation remained intact
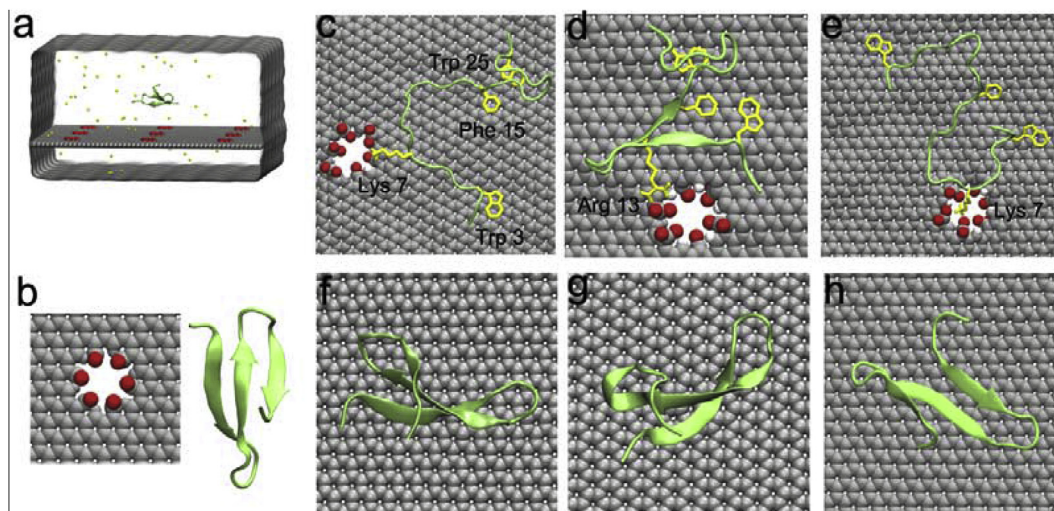
Fig. 1. (a) The initial system configuration where the YAP65WW protein is shown in the cartoon representation, the D-Gra sheet is shown as spheres (carbon, silver; oxygen, red; hydrogen, white), and the Na⁺ ions are colored in yellow spheres. The water box is rendered as a silver surface. (b) The structure of D-Gra with carboxyl groups and the crystal structure of YAP65WW. The representative contact configurations of YAP65WW protein adsorbed onto D-Gra (c–e) and I-Gra (f–h) surface. In (c–e), the key residues Trp-3, Trp-25, Arg-13, Phe-15 and Lys-7 that play key role in the binding process are labeled and highlighted by yellow sticks for clarity. (A colour version of this figure can be viewed online.)
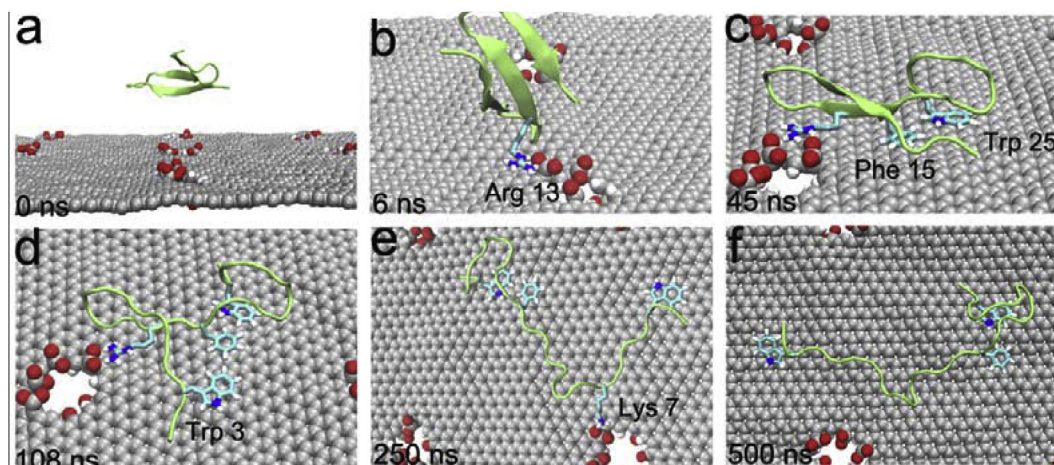

Fig. 2. Structural evolutions of YAP65WW protein on D-Gra surface in one representative simulation (run 1 in the following discussions). The TAP65WW is shown as cartoon. The atoms of D-Gra sheet are shown as spheres (C: gray spheres; O: red spheres; H: white spheres). The aromatic residues of Arg-13, Trp-25, Phe-15, Trp-3 and Lys-7 that play key role in the binding interface are shown as sticks. (A colour version of this figure can be viewed online.)

through the rest of the simulations. It should be noted that the other basic residue, Lys-7, formed a salt-bridge-like interaction with another defect in a more dynamic manner (Fig. 2e and f).

The structural changes of YAP65WW upon binding onto D-Gra and I-Gra were quantitatively assessed by calculating the root-mean-squared deviation (RMSD) of the heavy atoms with respect to the crystal structure and the results are summarized in Fig. 3. For the D-Gra (Fig. 3a), the large RMSD values indicate that YAP65WW experienced structural distortions upon binding to D-Gra. In contrast, the small RMSD values (Fig. 3b) on I-Gra simulation indicate that YAP65WW maintained its native structure mostly upon the adsorption onto I-Gra.

3.2. Secondary structure evolution of YAP65WW

Secondary structure evolution reveals complete YAP65WW β-sheet unfolding upon adsorption with defective graphene but not ideal graphene. For a more detailed analysis of structural changes to the YAP65WW domain during adsorption, we computed the secondary structure using the Define Secondary Structure of Proteins (DSSP) program [49]. In the native state, the YAP65WW domain has three antiparallel β-sheet segments: β-sheet 1 (residues 2–8), β-sheet 2 (residues 12–18) and β-sheet 3 (residues 21–25). Upon adsorption onto D-Gra (Fig. 4a), all three β-sheet segments unfold completely; only minor turns and bends remain at the end of the simulations. In contrast, the YAP65WW domain largely maintains its secondary structure after adsorption onto I-Gra, including most of the β-sheet segments (Fig. 4b).

Fig. 4d-e depicts the residual ratios of YAP65WW β-sheet after adsorption to the two graphene models. As can be seen in Fig. 4d, the β-sheet ratio of YAP65WW upon D-Gra adsorption quickly decreased to zero within 250 ns in traj-1 and traj-3. Traj-2, which demonstrated a more resilient conformation, unfolded around 380 ns though it continued to exhibit a fluctuating β-sheet ratio of 0–30%. In contrast, the β-sheet ratios of YAP65WW with I-Gra reveal that YAP65WW largely maintained its β-sheet structure
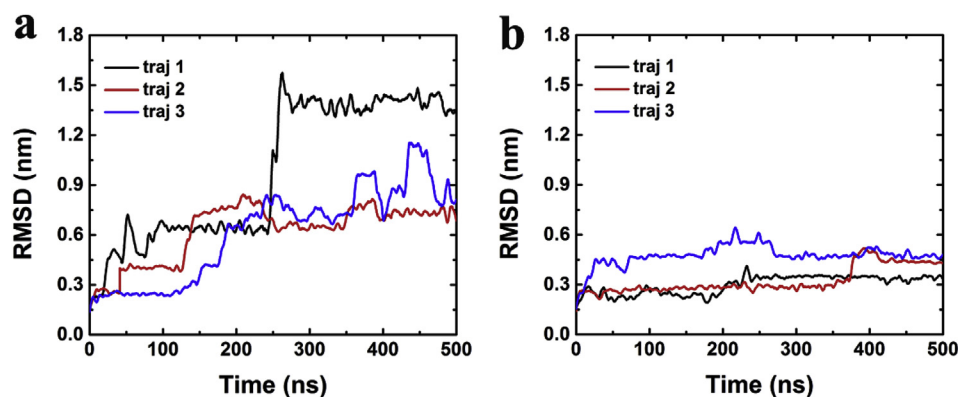
Fig. 3. Time evolution of the root-mean-squared deviation (RMSD) of the YAP65WW heavy atoms relative to the crystal structure upon binding to the surface of (a) D-Gra and (b) I-Gra. (A colour version of this figure can be viewed online.)
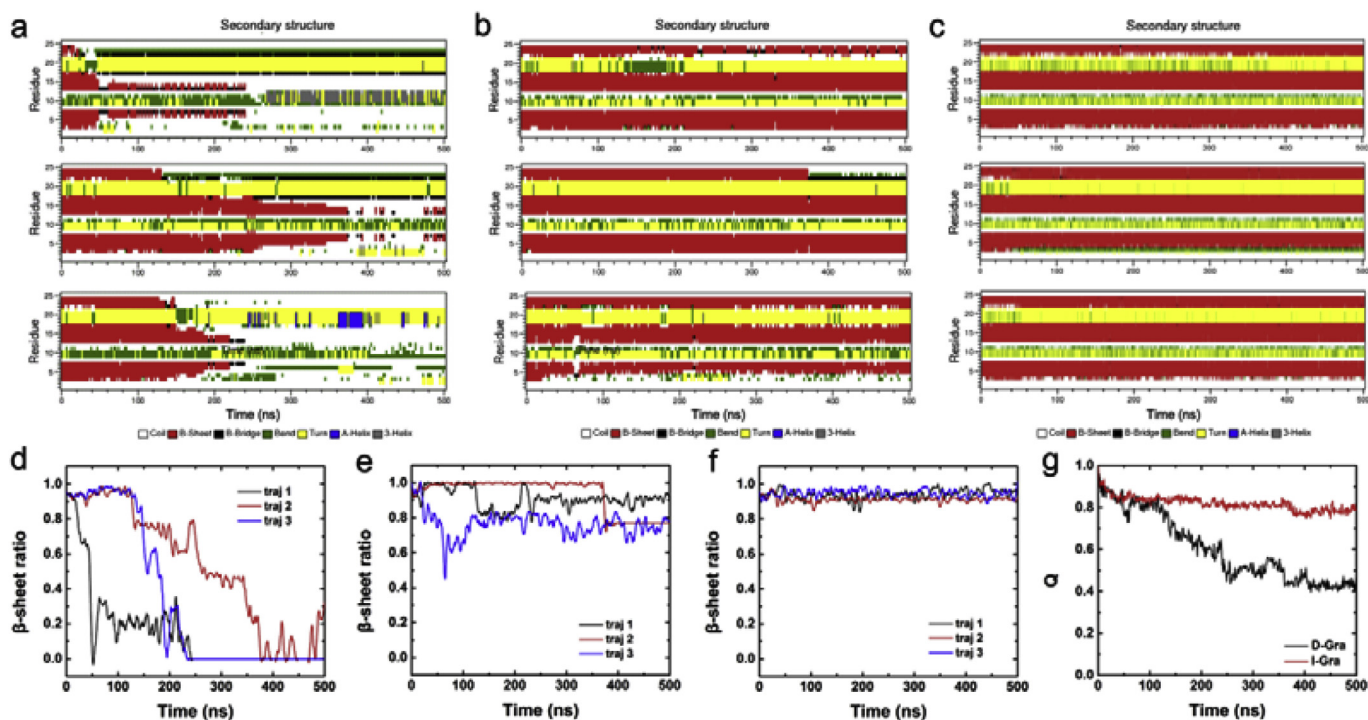

Fig. 4. Time evolution of the secondary structure of YAP65WW domain upon binding to the surface of (a) D-Gra, (b) I-Gra and (c) in water. Evaluations of β-sheet ratio with respect to crystal structure of YAP65WW on (d) D-Gra, (e) I-Gra and (f) in water from three independent trajectories. (g) The fraction of native protein contacts, Q, for YAP65WW domain upon binding to the D-Gra and I-Gra which are averaged over three trajectories. (A colour version of this figure can be viewed online.)

throughout the 500 ns trajectories, ending at 90%, 77% and 74% β-sheet, respectively (Fig. 4e). In order to show a reference of unabsorbed protein for comparison, we calculated the time evolution of the secondary structure and the β-sheet ratio of YAP65WW domain alone in water. As shown in Fig. 4c and f, the YAP65WW domain can well maintain its secondary structure during the 500 ns simulation time.

3.3. Tertiary structure evolution of YAP65WW

YAP65WW tertiary structure analysis reveals over half of tertiary contacts are destroyed upon binding to defective graphene compared to only 20% of contacts when binding to ideal graphene. To monitor the evolution of YAP65WW tertiary structure adsorbing onto D-Gra and I-Gra, we calculated the fraction of native protein

contacts over time, $Q(t)$. Following our previous work [50], $Q(t)$ is defined as the ratio of the total number of native contacts (using a distance cutoff of 0.5 nm) with respect to its native crystal structure at time t. Fig. 4g shows the time-resolved $Q(t)$ fraction averaged over the three defective and three ideal trajectories. The ideal graphene system lost about 20% of native contacts to reach a fraction of approximately 0.8 at 500 ns. However, for the defective graphene system, $Q(t)$ decreased to approximately 0.4 at 500 ns, meaning a 60% loss of native contacts. Ideal graphene's effect on YAP65WW tertiary structure was rather minor, breaking some native contacts but largely maintaining the same folded structure. In comparison, defective graphene broke three times as many native contacts as ideal graphene, resulting in a largely unfolded structure.

3.4. Binding characteristics of YAP65WW with two graphene structures

To characterize the loading process of YAP65WW on the two graphene models, we calculated the number of YAP65WW heavy atoms over time that are within 0.5 nm to D-Gra and I-Gra (abbreviated as N_{cont}), respectively. As depicted in Fig. 5a, the D-Gra-YAP65WW contact profile varies, but there are generally three stages that are observed: an initial stage of $N_{cont} = 20-50$ reached in a few nanoseconds, an intermediate stage with $N_{cont} = 80$, and a final stage of $N_{cont} = 110$. The final stage corresponds to fully unfolded structure of YAP65WW that forms intimate contacts with D-Gra as shown in the two insets of Fig. 5a. Interestingly, trajectory 2 never reaches the final stage, but remains steadfast at the intermediate stage of $N_{cont} = 80$. This agrees well with the secondary structure analysis that the trajectory 2 β-sheet profile never fully converges but fluctuates around 0—30%, indicating that trajectory 2 never transitions to the final contact number stage due to a slight but persistent β-sheet proclivity. For YAP65WW with I-Gra, the contact number analysis reveals just two stages: an initial stage of $N_{cont} = 20-40$ and a final stage of $N_{cont} = 60-80$. The ideal graphene sheet maintains fewer overall contacts with the YAP65WW protein than the defective graphene sheet. This is consistent with the secondary and tertiary structure analysis revealing that the YAP65WW protein in the I-Gra system remains largely folded while the YAP65WW in the D-Gra system unfolds, allowing buried residues to contact the D-Gra sheet resulting in higher contact numbers. In the insets of Fig. 5b, we draw two snapshots (150 ns in traj-1 and 250 ns in traj-2) of YAP65WW on I-Gra. These correspond to the initial stage of binding ($N_{cont} = 20-40$) where we observe YAP65WW binds to the graphene surface through the loops

between the β-sheets.

In order to further probe the thermodynamic origin of YAP65WW unfolding on D-Gra, the binding energy for YAP65WW/D-Gra and YAP65WW/I-Gra were calculated using the MM-PBSA method [51] where solvation effect was considered with a continuum model. All conformations from available simulation trajectories were included to improve the statistics (i.e., ensemble averages). These results are summarized in Table S3 in the SI. There is a distinct difference for the binding energetics between the YAP65WW/D-Gra and YAP65WW/I-Gra complex. The YAP65WW binding with D-Gra is considerably stronger than that with I-Gra, indicating the unfolded ensemble is more favorable in free energy on D-Gra (the protein is mostly folded on I-Gra). From energy decomposition analyses, we also found that the stronger binding was mainly due to the more favorable electrostatic attractions while vdW interactions also contributed.

We further calculated the contact probability of each residue in YAP65WW with D-Gra and I-Gra over all simulations. As shown in Fig. 5c, YAP65WW residues at the N-terminus and the loop between β-sheet 2 and 3 generally have higher contacting probabilities with ideal graphene than defective graphene. This is consistent with the binding snapshots in Fig. 5b that shows YAP65WW initially binds to I-Gra through its edges of the β-sheet. In contrast, β-sheet residues and residues in the loop between β-sheet 1 and 2 (residues 10, 11) as well as residues in the C-terminus (residues 25, 26) have higher contact probabilities with D-Gra than I-Gra. Notably, this binding pattern reflects charged residues binding to defective regions as well as hydrophobic residues binding to graphene surface, while the ideal graphene binding pattern only captures solvent exposed residues (surface residues) binding to the graphene surface. Aromatic, π—π stacking interactions are known
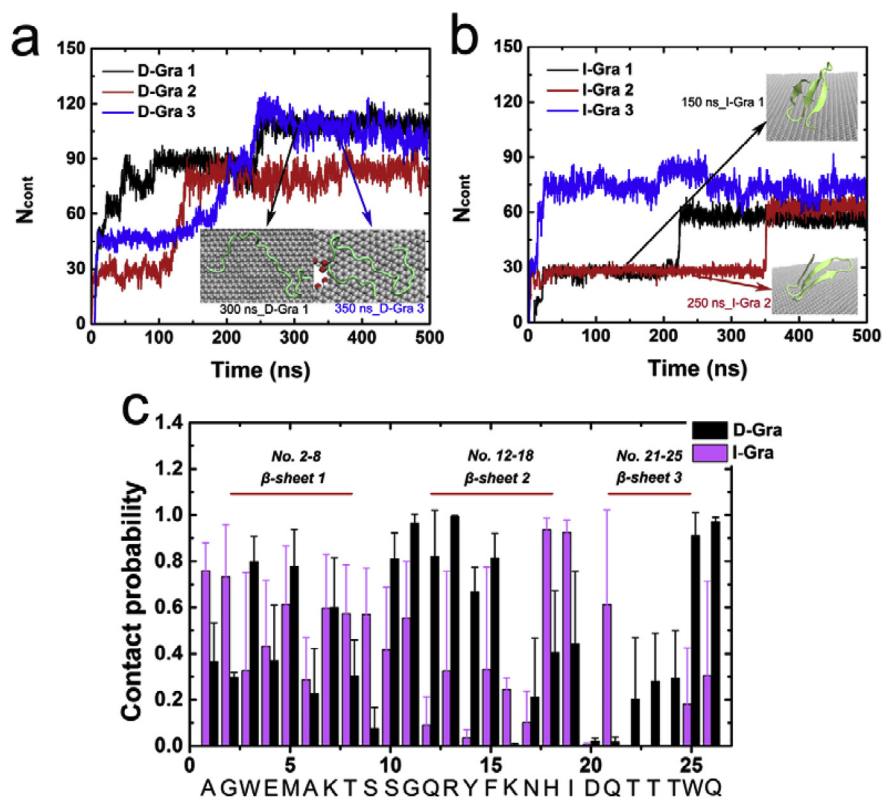

Fig. 5. (a—b) Time-resolved contact number between YAP65WW and D-Gra (a) and I-Gra (b) over the three trajectories, respectively. (c) The contact probability of each residue in YAP65WW protein with the surface of D-Gra and I-Gra. For (c), contacts are averaged over three trajectories in the respective system and the error bars indicate standard deviations. (A colour version of this figure can be viewed online.)
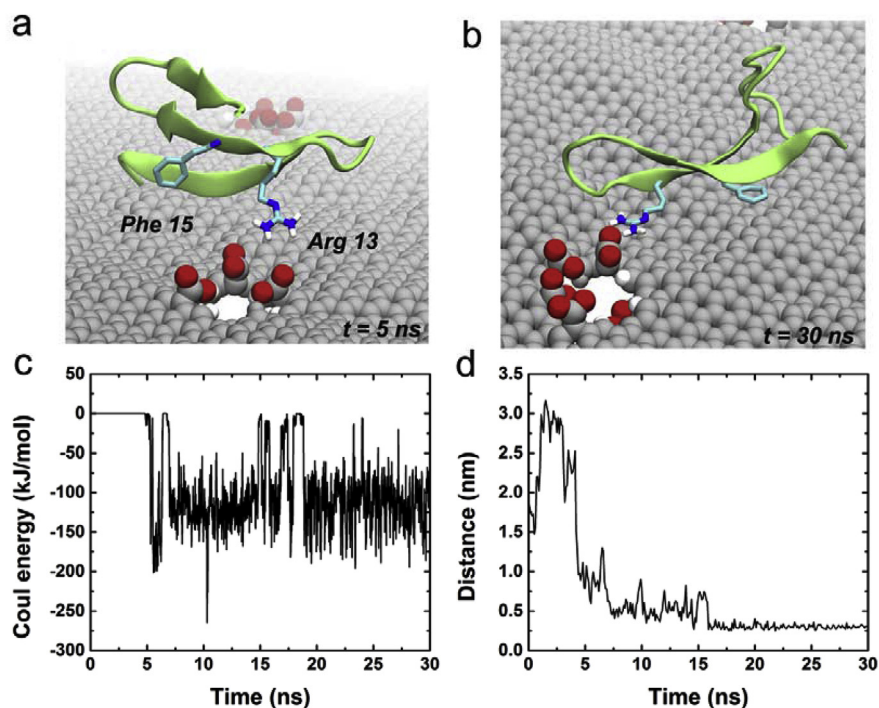
Fig. 6. Representative snapshots showing the formation of (a) Coulombic interactions between Arg-13 and the defect carboxyl group and (b) the π-π stacking interactions between Phe-15 and graphene. (c) Evolution of the Coulombic energy between the residue Arg-13 and the defect carboxyl group during the first 30 ns simulation. (d) Evolution of the minimum distance of Phe-15 from the surface of D-Gra. (A colour version of this figure can be viewed online.)

to be very important in proteins adsorbing onto the *sp* [2] hybridized carbon of graphene [33,40,52,53]. In our systems, the defective graphene is observed to unfold YAP65WW, exposing buried aromatic residues which then form favorable graphene interactions (more below). These favorable interactions are observed less in the ideal graphene system, as the protein remains intact, keeping those aromatic residues buried. In particular, aromatic residues Trp 3, Tyr 14 and Trp 25 have much higher contact probability with D-Gra than with I-Gra. It is noted that the Lys-7 residue also plays a role for YAP65WW unfolding as depicted in Fig. 2e, but its contact probability with D-Gra is as same as that with I-Gra. This is because Lys-7 can only form temporary binding with the defects in D-Gra, which is not as strong as Arg-13. After a period of simulation time, it can depart from the defect as shown in Fig. 2f. For the case of Arg-13, in addition to the favorable electrostatic attractions, the binding is further strengthened by arginine's relatively large planar guanidinium group which can form strong van der Waals interactions with aromatic rings on graphene.

It is well known that the interface water can effectively mediate interactions between protein and nanomaterials. Here, we studied the water distribution around YAP65WW to show the effect of interlayer water in regulating the interactions with defective graphene (see SI Fig. S2). We highlighted two representative residues, Arg-13 (the most important residue in initial anchoring) and Phe-15 (one of the mostly buried aromatic residue) for illustration. The water population in the first solvation shell (FSS) of both residues was noticeably affected once in contact with the D-Gra. For Arg-13, it formed strong Coulombic interactions with the carboxylate group in the defect, resulting in a loss of ~8 interfacial water molecules (Fig. S2 a-b). These water molecules played as a "mediator" for the Arg-Carboxylate slat bridge. Meanwhile, Phe-15 lost ~10 interfacial water molecules once exposed and in contact with D-Gra (on the *sp2* domain part and forming π-π stacking), due to the favorable "nanoscale dewetting" (Fig. S2 c-d), which provides

strong hydrophobic driving force for the binding [54—56]. On the other hand, the protein stays largely folded on I-Gra with slippery motions on the surface, showing no significant effects from the interfacial water molecules in this case (both Arg-13 and Phe-15 display roughly the same FSS water molecules before or after contacting I-Gra).

Fig. 6 supports the role of charged and aromatic interactions in YAPA65WW adsorbing to defective graphene. At 5 ns, the secondary structure of YAP65WW is still well maintained. The Arg-13 has established interactions with the negatively charged carboxyl groups at the defect edge, while Phe-15 is away from the D-Gra. At 30 ns, β-sheet 3 has completely unfolded, exposing Phe-15 which forms π−π stacking interactions with D-Gra. Throughout this process, the Arg-13 remains firmly anchored at the defect. We quantified this resilient Coulombic interaction between D-Gra and the Arg-13 as shown in Fig. 6c. The corresponding distance between Phe-15 and D-Gra surface was also calculated and presented in Fig. 6d. At the beginning of simulation, Arg-13 did not contact D-Gra. At t = ~5 ns, Arg-13 quickly approached the defect region of D-Gra, and the Coulombic interaction energy decreased dramatically from 0 kJ/mol to −200 kJ/mol. Admittedly, this decrease in energy is biased because of the absence of solvent screening in our calculation; however, it still indicates favorable Coulombic attraction, which we observed to restrict Arg-13 movement. Meanwhile, Phe-15 fluctuates from 3.0 nm separation distance from D-Gra to 0.8 nm at t = 5 ns. At this point, it is clear there are favorable hydrophobic interactions between Phe-15 and D-Gra, as the separation distance continues to decrease until reaching a value of 0.3 nm by 21 ns. More importantly, while the Arg-13 is restricted at the defect region (acting as an "anchor"), the rest of the protein can still migrate easily along the transverse directions along graphene surface (as can be seen from Fig. 6a to b). From these results, we observe that the unfolding of β-sheet 3 is mainly caused by a "diffusion-mismatch" between the Arg-13 (small diffusion) and the

other part of YAP65WW (large diffusion). The movements of the rest of the protein around the pivotal anchors create an "effective centripetal force" to the anchoring residues such as Arg-13. This effective centripetal force or stretching can cause the disruption of the native intra-protein interactions (i.e. native contacts) that maintain protein structure, thus resulting in local unfolding.

To evaluate the effect of defects on residue diffusions, we further simulated the binding process of two small dipeptide models (sequence: Lys-Phe and Arg-Phe) on I-Gra and D-Gra respectively. The diffusive motions are estimated using the Einstein relation. The results are summarized in Table S3 in the SI from which severe diffusive suppression have been observed for both Lys-Phe and Arg-Phe dipeptides on D-Gra. From these results, it can be deduced that there exist a "diffusion mismatch" for anchoring residues at the defects and residues at the other parts of the protein.

4. Conclusion

We investigated the adsorption of the WW-domain (YAP65WW) protein onto defective and ideal graphene layers by molecular dynamics simulation. While YAP65WW maintained its structural integrity on ideal graphene, severe disruption was observed for YAP65WW binding with defective graphene. This is driven by strong Coulombic interactions between the positively charged residues of YAP65WW and the negatively charged graphene defects. Through thermal movements of the other parts of the YAP65WW protein, local unfolding near the immobilized residues occurs, exposing buried aromatic residues which are observed to form favorable π-π interactions with the graphene surface and further extend the protein denaturation. Essentially, we observe detrimental protein unfolding only when the YAP65WW protein binds to defective graphene and not ideal graphene. Our work highlights the importance of understanding nanomaterial defects and their roles in nano-bio interactions and nanotoxicity.

Acknowledgement

Appendix A. Supplementary data

Supplementary data to this article can be found online at https://doi.org/10.1016/j.carbon.2019.01.107.

References

[1] J.R. Williams, L. DiCarlo, C.M. Marcus, Quantum Hall effect in a gate-controlled P-N junction of graphene, Science 317 (2007) 638—641.

[2] C. Lee, X.D. Wei, J.W. Kysar, J. Hone, Measurement of the elastic properties and intrinsic strength of monolayer graphene, Science 321 (2008) 385—388.

[3] D.K. Palit, A.V. Sapre, J.P. Mittal, C.N.R. Rao, Photophysical properties of the fullerenes, C-60 and C-70, Chem. Phys. Lett. 195 (1992) 1—6.

[4] D.E.H. Jones, Science of fullerenes and carbon nanotubes - dresselhaus,Ms, dresselhaus,G, Eklund,Pc, Nature 381 (1996), 384-384.

[5] V.C. Sanchez, A. Jachak, R.H. Hurt, A.B. Kane, Biological interactions of graphene-family nanomaterials: an interdisciplinary review, Chem. Res. Toxicol. 25 (2012) 15—34.

[6] H.Q. Bao, Y.Z. Pan, Y. Ping, N.G. Sahoo, T.F. Wu, L. Li, J. Li, L.H. Gan, Chitosan-functionalized graphene oxide as a nanocarrier for drug and gene delivery, Small 7 (2011) 1569—1578.

[7] A.A. Bhirde, V. Patel, J. Gavard, G.F. Zhang, A.A. Sousa, A. Masedunskas,

R.D. Leapman, R. Weigert, J.S. Gutkind, J.F. Rusling, Targeted killing of cancer cells in vivo and in vitro with egf-directed carbon nanotube-based drug delivery, ACS Nano 3 (2009) 307—316.

[8] X.M. Sun, Z. Liu, K. Welsher, J.T. Robinson, A. Goodwin, S. Zaric, H.J. Dai, Nano-graphene oxide for cellular imaging and drug delivery, Nano Research 1 (2008) 203—212.

[9] Y.K. Kim, H.K. Na, S.J. Kwack, S.R. Ryoo, Y. Lee, S. Hong, S. Hong, Y. Jeong, D.H. Min, Synergistic effect of graphene oxide/mwcnt films in laser desorption/ionization mass spectrometry of small molecules and tissue imaging, ACS Nano 5 (2011) 4550—4561.

[10] Z. Liu, S. Tabakman, S. Sherlock, X.L. Li, Z. Chen, K.L. Jiang, S.S. Fan, H.J. Dai, Multiplexed five-color molecular imaging of cancer cells and tumor tissues with carbon nanotube Raman tags in the near-infrared, Nano Research 3 (2010) 222—233.

[11] J.T. Robinson, S.M. Tabakman, Y.Y. Liang, H.L. Wang, H.S. Casalongue, D. Vinh, H.J. Dai, Ultrasmall reduced graphene oxide with high near-infrared absorbance for photothermal therapy, J. Am. Chem. Soc. 133 (2011) 6825—6831.

[12] H.W. Yang, et al., Egrf conjugated pegylated nanographene oxide for targeted chemotherapy and photothermal therapy, Biomaterials 34 (2013) 7204—7214.

[13] B. Tian, C. Wang, S. Zhang, L.Z. Feng, Z. Liu, Photothermally enhanced photodynamic therapy delivered by nano-graphene oxide, ACS Nano 5 (2011) 7000—7009.

[14] L. Ma-Hock, S. Treumann, V. Strauss, S. Brill, F. Luizi, M. Mertler, K. Wiench, A.O. Gamer, B. van Ravenzwaay, R. Landsiedel, Inhalation toxicity of multiwall carbon nanotubes in rats exposed for 3 months, Toxicol. Sci. 112 (2009) 468—481.

[15] C.A. Poland, R. Duffin, I. Kinloch, A. Maynard, W.A.H. Wallace, A. Seaton, V. Stone, S. Brown, W. MacNee, K. Donaldson, Carbon nanotubes introduced into the abdominal cavity of mice show asbestos-like pathogenicity in a pilot study, Nat. Nanotechnol. 3 (2008) 423—428.

[16] L.A. Mitchell, F.T. Lauer, S.W. Burchiel, J.D. McDonald, Mechanisms for how inhaled multiwalled carbon nanotubes suppress systemic immune function in mice, Nat. Nanotechnol. 4 (2009) 451—456.

[17] Z. Li, T. Hulderman, R. Salmen, R. Chapman, S.S. Leonard, S.H. Young, A. Shvedova, M.I. Luster, P.P. Simeonova, Cardiovascular effects of pulmonary exposure to single-wall carbon nanotubes, Environ. Health Perspect. 115 (2007) 377—382.

[18] J. Kolosnjaj, H. Szwarc, F. Moussa, Toxicity studies of carbon nanotubes, Adv. Exp. Med. Biol. 620 (2007) 181—204.

[19] A.E. Porter, M. Gass, K. Muller, J.N. Skepper, P.A. Midgley, M. Welland, Direct imaging of single-walled carbon nanotubes in cells, Nat. Nanotechnol. 2 (2007) 713—717.

[20] K.H. Park, M. Chhowalla, Z. Iqbal, F. Sesti, Single-walled carbon nanotubes are a new class of ion channel blockers, J. Biol. Chem. 278 (2003) 50212—50216.

[21] M. Calvaresi, S. Furini, C. Domene, A. Bottoni, F. Zerbetto, Blocking the passage: C-60 geometrically clogs K+ channels, ACS Nano 9 (2015) 4827—4834.

[22] Y.S. Tu, et al., Destructive extraction of phospholipids from Escherichia coli membranes by graphene nanosheets, Nat. Nanotechnol. 8 (2013) 594—601.

[23] X. Liu, G.X. Duan, W.F. Li, Z.F. Zhou, R.H. Zhou, Membrane destruction-mediated antibacterial activity of tungsten disulfide (Ws2), RSC Adv. 7 (2017) 37873—37880.

[24] A. Nourbakhsh, M. Cantoro, T. Vosch, G. Pourtois, F. Clemente, M.H. van der Veen, J. Hofkens, M.M. Heyns, S. De Gendt, B.F. Sels, Bandgap opening in oxygen plasma-treated graphene, Nanotechnology 21 (2010).

[25] S. Garaj, W. Hubbard, A. Reina, J. Kong, D. Branton, J.A. Golovchenko, Graphene as a subnanometre trans-electrode membrane, Nature 467 (2010), 190-U73.

[26] Y. You, J. Deng, X. Tan, N. Gorjizadeh, M. Yoshimura, S.C. Smith, V. Sahajwalla, R.K. Joshi, On the mechanism of gas adsorption for pristine, defective and functionalized graphene, Phys. Chem. Chem. Phys. 19 (2017) 6051—6056.

[27] P. Cabrera-Sanfelix, Adsorption and reactivity of Co2 on defective graphene sheets, J. Phys. Chem. 113 (2009) 493—498.

[28] F. De Leo, A. Magistrato, D. Bonifazi, Interfacing proteins with graphitic nanomaterials: from spontaneous attraction to tailored assemblies, Chem. Soc. Rev. 44 (2015) 6916—6953.

[29] Z.Y. Wang, W.P. Zhu, Y. Qiu, X. Yi, A. von dem Bussche, A. Kane, H.J. Gao, K. Koski, R. Hurt, Biological and environmental interactions of emerging two-dimensional nanomaterials, Chem. Soc. Rev. 45 (2016) 1750—1780.

[30] J.J. Guo, X.J. Yao, L.L. Ning, Q.Q. Wang, H.X. Liu, The adsorption mechanism and induced conformational changes of three typical proteins with different secondary structural features on graphene, RSC Adv. 4 (2014) 9953—9962.

[31] M. Sudol, K. Sliwa, T. Russo, Functions of ww domains in the nucleus, FEBS Lett. 490 (2001) 190—195.

[32] R.J. Ingham, et al., Ww domains provide a platform for the assembly of multiprotein networks, Mol. Cell Biol. 25 (2005) 7092—7106.

[33] G.H. Zuo, Q. Huang, G.H. Wei, R.H. Zhou, H.P. Fang, Plugging into proteins: poisoning protein function by a hydrophobic nanoparticle, ACS Nano 4 (2010) 7508—7514.

[34] Y. Ling, Z.L. Gu, S.G. Kang, J.D. Luo, R.H. Zhou, Structural damage of a beta-sheet protein upon adsorption onto molybdenum disulfide nanotubes, J. Phys. Chem. C 120 (2016) 6796—6803.

[35] M.J. Macias, M. Hyvonen, E. Baraldi, J. Schultz, M. Sudol, M. Saraste, H. Oschkinat, Structure of the ww domain of a kinase-associated protein complexed with a proline-rich peptide, Nature 382 (1996) 646—649.

[36] A.D. MacKerell, et al., All-atom empirical potential for molecular modeling and

dynamics studies of proteins, J. Phys. Chem. B 102 (1998) 3586–3616.

[37] W. Humphrey, A. Dalke, K. Schulten, Vmd: visual molecular dynamics, J. Mol. Graph. Model. 14 (1996) 33–38.

[38] G. Hummer, J.C. Rasaiah, J.P. Noworyta, Water conduction through the hydrophobic channel of a carbon nanotube, Nature 414 (2001) 188–190.

[39] X.J. Gong, J.Y. Li, H.J. Lu, R.Z. Wan, J.C. Li, J. Hu, H.P. Fang, A charge-driven molecular water pump, Nat. Nanotechnol. 2 (2007) 709–712.

[40] G. Zuo, X. Zhou, Q. Huang, H.P. Fang, R.H. Zhou, Adsorption of villin headpiece onto graphene, carbon nanotube, and C60: effect of contacting surface curvatures on binding affinity, J. Phys. Chem. C 115 (2011) 23323–23328.

[41] W.L. Jorgensen, J. Chandrasekhar, J.D. Madura, R.W. Impey, M.L. Klein, Comparison of simple potential functions for simulating liquid water, J. Chem. Phys. 79 (1983) 926–935.

[42] B. Hess, C. Kutzner, D. van der Spoel, E. Lindahl, Gromacs 4: algorithms for highly efficient, load-balanced, and scalable molecular simulation, J. Chem. Theor. Comput. 4 (2008) 435–447.

[43] T. Darden, D. York, L. Pedersen, Particle mesh Ewald - an N.log(N) method for Ewald sums in large systems, J. Chem. Phys. 98 (1993) 10089–10092.

[44] U. Essmann, L. Perera, M.L. Berkowitz, T. Darden, H. Lee, L.G. Pedersen, A smooth particle mesh Ewald method, J. Chem. Phys. 103 (1995) 8577–8593.

[45] B. Hess, H. Bekker, H.J.C. Berendsen, J. Fraaije, Lincs: a linear constraint solver for molecular simulations, J. Comput. Chem. 18 (1997) 1463–1472.

[46] G. Bussi, D. Donadio, M. Parrinello, Canonical sampling through velocity rescaling, J. Chem. Phys. 126 (2007).

[47] H.J.C. Berendsen, J.P.M. Postma, W.F. Vangunsteren, A. Dinola, J.R. Haak, Molecular-dynamics with coupling to an external bath, J. Chem. Phys. 81 (1984) 3684–3690.

[48] Z. Gu, W. Li, L. Hong, R. Zhou, Exploring biological effects of Mos2 nanosheets on native structures of alpha-helical peptides, J. Chem. Phys. 144 (2016), 175103-175103.

[49] W. Kabsch, C. Sander, Dictionary of protein secondary structure - pattern-recognition of hydrogen-bonded and geometrical features, Biopolymers 22 (1983) 2577–2637.

[50] B.Y. Li, W.F. Li, J.M. Perez-Aguilar, R.H. Zhou, Mild binding of protein to C2n monolayer reveals its suitable biocompatibility, Small 13 (2017).

[51] R. Kumari, R. Kumar, A. Lynn, O.S.D.D. Consort, G_Mmpbsa-a gromacs tool for high-throughput mm-pbsa calculations, J. Chem. Inf. Model. 54 (2014) 1951–1962.

[52] G.H. Zuo, W. Gu, H.P. Fang, R.H. Zhou, Carbon nanotube wins the competitive binding over proline-rich motif ligand on Sh3 domain, J. Phys. Chem. C 115 (2011) 12322–12328.

[53] C.C. Ge, et al., Binding of blood proteins to carbon nanotubes reduces cytotoxicity, P Natl Acad Sci USA 108 (2011) 16968–16973.

[54] P. Das, D. Kapoor, K.T. Halloran, R. Zhou, C.R. Matthews, Interplay between drying and stability of a tim barrel protein: a combined simulation-experimental study, J. Am. Chem. Soc. 135 (2013) 1882–1890.

[55] P. Liu, X. Huang, R. Zhou, B.J. Berne, Observation of a dewetting transition in the collapse of the melittin tetramer, Nature 437 (2005) 159–162.

[56] R. Zhou, X. Huang, C.J. Margulis, B.J. Berne, Hydrophobic collapse in multi-domain protein folding, Science 305 (2004) 1605–1609.